RSC Advances

PAPER

View Article Online
View Journal | View Issue

Cite this: *RSC Adv.*, 2017, **7**, 33745

Enhancing the rate performance of spherical $LiFeBO_3/C$ *via* Cr doping

X. X. Dong, C. Y. Huang, Q. Jin, J. Zhou, P. Feng, F. Y. Shi and D. Y. Zhang *

Spherical $LiFe_{1-x}Cr_xBO_3/C$ (x = 0, 0.005, 0.008) has been successfully synthesized by ball-milling and spray-drying assisted high-temperature solid-state reaction. The effect of Cr doping on $LiFeBO_3/C$ is characterized by XRD, energy-dispersive X-ray spectroscopy (EDS) and XPS. The results show that $LiFe_{0.995}Cr_{0.005}BO_3/C$ delivers the highest initial discharge specific capacity of 196.3 mA h g^{-1} at 0.1C and superior rate capability of 90 mA h g^{-1} at 5C. Moreover the material presents a cyclic retention of 95% after 50 cycles at 1C. Such improvement in the electrochemical performance can be attributed to the high electronic conductivities (4.75×10^{-5} S cm^{-1}) and Li ion diffusion coefficients (9.20×10^{-13} cm^2 s^{-1}). The introduction of supervalent Cr^{3+} into the $LiFeBO_3$ lattice produces Fe vacancies with accompanying conduction electrons, which lead to the enhanced electronic conductivity and Li ion diffusion coefficient.

Received 14th March 2017
Accepted 22nd June 2017

DOI: 10.1039/c7ra03028b

rsc.li/rsc-advances

1. Introduction

In recent years olivine $LiFePO_4$ has been deeply researched and dominates most vehicle markets due to its safety, potentially low cost and environmental benignity, but the low theoretical capacity of $LiFePO_4$ cannot sufficiently meet the requirements for high-energy density applications. Besides phosphates, the other polyanion-type cathode materials, including borates, silicates and titanates, have attracted great attention.[1–7] Among them, $LiFeBO_3$ has been regarded as a promising cathode alternative for lithium ion batteries due to its higher theoretical capacity (220 mA h g^{-1}), higher electrical conductivity (3.9×10^{-7} S cm^{-1}) and smaller volume change (2%) than those of the $LiFePO_4$.

The electrochemical performance of $LiFeBO_3$ was firstly reported by Legagneur *et al.*, and the poor electrical conductivity and low ionic conductivity of the pristine $LiFeBO_3$ hindered its performance.[8] Yamada *et al.* made great progress in the electrochemical performance of $LiFeBO_3$, which arrived at a capacity of >190 mA h g^{-1} at 0.05C, by introducing ketchen black and vapor grown carbon fibers to increase its electrical conductivity.[9] They claimed that the significant positive impact was realized by avoiding the surface poisoning of $LiFeBO_3$ resulting from contact with moisture in the air. Meanwhile, Khalifah *et al.* demonstrated that the moisture in the air may poison the surface of $LiFeBO_3$ particles and induce severe degradation of electrochemical properties.[10] Carbon coating was proved to enhance the electrical conductivity of $LiFeBO_3$ as well as prevent it from air exposure.[4,11,12] Multi-layer core–shell structural $LiFeBO_3/C$, synthesized by sol–gel method, presented an initial discharge specific capacity of 196.5 mA h g^{-1} at 0.05C, which dropped to 136.1 mA h g^{-1} after 30 cycles.[4] Moreover, its discharge specific capacity dropped to 120 mA h g^{-1} at 0.25C. Thus, the rate and cycle performance were considered to be severe challenges. Both particle size reducing and cation doping methods were investigated to improve the electrochemical performance of $LiFeBO_3$.[13–17] Recently, Chen *et al.* reported that nano-sized $LiFeBO_3/C$ mesoporous hollow spheres delivered not only a high initial reversible capacity of 190 mA h g^{-1} at 0.05C, but also superior rate capability (80 mA h g^{-1}) up to 4C, even delivered a discharge capability of 69 mA h g^{-1} at 8C.[13] It was attributed to the high Li ion diffusion resulting from its nano-size particles, high surface area and large pore volume. The similar results also had been reported by Zhang *et al.* about nano-sized $LiMnBO_3/C$.[14] Yamada and co-workers found that the electrochemical properties of $Li(Mn_xFe_{1-x})BO_3$ decreased with the Mn content increasing.[15] The result was not consistent with the expected. Cation doping had been proved to be an efficient way to increase the rate performance of $LiFePO_4$.[18–21] Wang *et al.* reported that the rate capability and cyclic stability of $LiFePO_4$ were greatly enhanced by bivalent cation (Ni, Co or Mg) doping at Fe-site.[18] They attributed the significant improvement in electrochemical performance to the enhanced electronic conductivities and probably the mobility of Li ions in the doped samples. Park *et al.* noted Cr doping facilitates Li ion diffusion during the charge–discharge cycles.[19] However, few works had been done to improve the rate performance of $LiFeBO_3$ by Cr doping.

In this paper, $LiFe_{1-x}Cr_xBO_3/C$ (x = 0, 0.005, 0.008) was prepared by ball-milling and spray-drying assisted high-temperature solid-state reaction. Ball-milling is an effective

School of Material Science and Engineering, Shanghai Institute of Technology, Shanghai 201418, China. E-mail: dyz@sit.edu.cn

method for obtaining homogeneous mixture of raw materials and controlling the size of primary particle. Spray-drying is easy to obtain spherical particles. Ball-milling and spray-drying technique offers a simple, cheap and a robust way to prepare $LiFeBO_3$/C. The effects of Cr doping on the electrochemical properties of $LiFeBO_3$ were investigated.

2. Experimental

The $LiFe_{1-x}Cr_xBO_3$/C (x = 0, 0.005, 0.008) samples were synthesized by a solid-state reaction. $LiOH\cdot H_2O$, $FeC_2O_4\cdot 2H_2O$, H_3BO_3, Cr_2O_3 and caramel were used as raw materials. All raw materials were mixed by ball milling at a speed of 600 rpm for 3 h with 0.4 mm ZrO_2 beads as the grinding media, and finally a green suspension was generated. Then, the suspension was dried by a spray dryer and spherical precursor was obtained. At last, the as-prepared precursor were transferred into a tube furnace and sintered at 550 °C for 7 h under the N_2 atmosphere to yield $LiFe_{1-x}Cr_xBO_3$/C (x = 0, 0.005, 0.008) samples.

Phase identification was performed by X-ray powder diffraction measurement (XRD, Bruker D8 Focus diffractometer) with Cu Kα radiation (0.1541 nm) at a scanning rate of 0.01° per second in the 2θ range from 10° to 70°. The morphologies of the samples were monitored by a scanning electron microscope (SEM, JEOL, JSM-6700F) and a transmission electron microscope (TEM, JEOL JEM-2100). The chemical composition was determined by energy dispersive X-ray spectroscopy (EDS, Bruker, XFlash 4010). X-ray photoelectron spectroscopy (XPS, Kratos Axis Ultra DLD) with Al Kα radiation was employed to measure the state of each element in the surface. Elemental carbon analysis of sample was performed by C–S analysis equipment (HIR-944B). The electronic conductivities of the cylindrical pellets with a diameter of 10 mm of the synthesized samples were measured at room temperature using a powder resistivity tester (FT-300/301) under a pressure range of 2 to 22 MPa and a resistivity range of 10^{-4} Ω cm to 2×10^5 Ω cm.

The electrochemical characterizations were performed using CR2016 coin-type cell. The working electrodes were fabricated by mixing the active material ($LiFe_{1-x}Cr_xBO_3$/C, x = 0, 0.005, 0.008), super P and polyvinylidene fluoride (PVDF) binder in a weight ratio of 8 : 1 : 1 in *N* methyl-2-pyrrolidone (NMP). The mixed slurry was coated uniformly on aluminium foil, dried in the vacuum for 4 h at 120 °C. Then electrodes pressed into pellets of 12 mm in diameter where about 6 mg of active materials was hold on it. Two-electrode electrochemical cells were assembled in a glove box filled with high-purity argon where $LiFe_{1-x}Cr_xBO_3$/C (x = 0, 0.005, 0.008) electrodes as a cathode, the lithium metal foil was used as an anode, Celgard2320 as separator and 1 M $LiPF_6$ in EC : DMC (1 : 1 vol%) were used as an electrolyte. The electrochemical measurements were performed by Land Battery Testers (LAND-CT2001A) in the voltage range between 1.5 and 4.5 V. Constant-current and constant-voltage (CC–CV) charging methods were used to measure the capacity of $LiFe_{1-x}Cr_xBO_3$/C (x = 0, 0.005, 0.008). The cells were first galvanostatically charged at 0.1C (1C = 220 mA g^{-1}) to 4.5 V, then charged at constant voltage of 4.5 V until the current decay below 0.05C, finally the cells were discharged to 1.5 V at a current rate of 0.1C. The rate performance was performed by charging and discharging at various rates ranging from 0.1C to 5C. The electrochemical impedance spectroscopy (EIS) measurements were conducted using electrochemical workstation (Autolab PGSTAT302N). The frequency range was 10^{-2} to 10^5 Hz, and the amplitude was 5 mV. It should be pointed out that all the electrochemical measurements were performed at room temperature (25 °C).

3. Results and discussion

Fig. 1(a) shows the XRD patterns of all the $LiFe_{1-x}Cr_xBO_3$/C (x = 0, 0.005, 0.008) samples. Compared with the XRD pattern of the $LiFeBO_3$/C sample, the XRD patterns of the Cr-doped samples do not exhibit extra reflections. All of the diffraction peaks of the samples could be indexed into the monoclinic $LiFeBO_3$ (PDF card #00-054-0026) with space group of *C*2/*c*. Fig. 1(b) shows the peak shift toward larger angles in the XRD data induced by Cr doping, which indicated the change of the lattice parameter. The lattice parameters of the $LiFe_{1-x}Cr_xBO_3$/C (x = 0, 0.005, 0.008) samples are calculated by MDI Jade 9.0 software, and the results are listed in Table 1. As can be seen from the Table 1, the unit cell volume of $LiFeBO_3$/C is contract with the increasing of Cr doping. The radius of Cr (0.64 Å) is smaller than that of Fe (0.74 Å). Thus, the lattice contracted after Cr doping, which is in accordance with the results reported by Gan *et al.*

The morphology of the $LiFe_{0.995}Cr_{0.005}BO_3$/C sample was observed *via* SEM, as shown in Fig. 2(a) and (b) presents similar spherical particles with a size distribution ranging from 5 μm to 10 μm. As shown in Fig. 2(c), the spherical particles are actually an aggregation of a lot of smaller primary particles. Fig. 2(d) shows an enlarged image of the $LiFe_{0.995}Cr_{0.005}BO_3$/C sample. The surface of the primary particles may covered by gel-liked carbon, which forms a network among primary particles to improve the electrical conductivity of the sample. Furthermore,

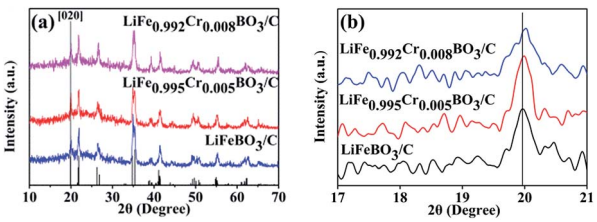

Fig. 1 (a) XRD patterns of $LiFe_{1-x}Cr_xBO_3$ (x = 0, 0.005, 0.008); (b) the peak shift of [020] lattice plane.

Table 1 Lattice parameters of the $LiFe_{1-x}Cr_xBO_3$/C (x = 0, 0.005, 0.008)

Sample	a (nm)	b (nm)	c (nm)	V (nm^3)
x = 0	0.51533	0.89074	1.01946	0.4679
x = 0.005	0.51524	0.89065	1.01895	0.4675
x = 0.008	0.51479	0.88853	1.02121	0.4670

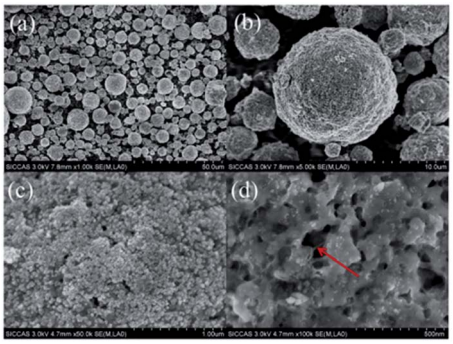

Fig. 2 (a and b) Low-magnification and (c and d) high-magnification SEM images of the $LiFe_{0.995}Cr_{0.005}BO_3/C$.

there are a large number of micro pores among the primary particles. This microporous structure can provide sufficient space for electrolyte penetrating and increase the electrode–electrolyte interface area, which may enhance the Li ion diffusion coefficient. So the $LiFe_{0.995}Cr_{0.005}BO_3/C$ sample tends to deliver excellent electrochemical performance.

A Bruker-AXS 133 eV XFlash 4010 Detector attached to the SEM is used to observe the elemental distribution of $LiFe_{0.995}Cr_{0.005}BO_3/C$. As shown in Fig. 3, different colours represent different elements. The results illustrate that the elements (O, Cr and Fe) are uniformly distributed in the $LiFe_{0.995}Cr_{0.005}BO_3/C$ samples. Combined with the XRD results, it can be inferred that the Cr probably enters the structure of $LiFeBO_3$ to form a solid solution.

To observe the morphology of carbon layer of the $LiFe_{0.995}Cr_{0.005}BO_3/C$, TEM images are presented in Fig. 4. As shown in Fig. 4(a), the darker spherical particles are well wrapped by flocculent layer. According to the further enlarged image as shown Fig. 4(b), the *d* spacing value (0.4406 nm) in the darker spherical particles consist with the [011] lattice spacing of $LiFeBO_3$, which indicates the sample are highly crystalline. The flocculent layer is contributed to amorphous carbon. This amorphous carbon layer may prevent $LiFe_{0.995}Cr_{0.005}BO_3/C$ from surface poisoning when it exposed in the moisture air. The amount of carbon in the $LiFe_{0.995}Cr_{0.005}BO_3/C$ is about 3.0 wt% determined by C–S analysis method.

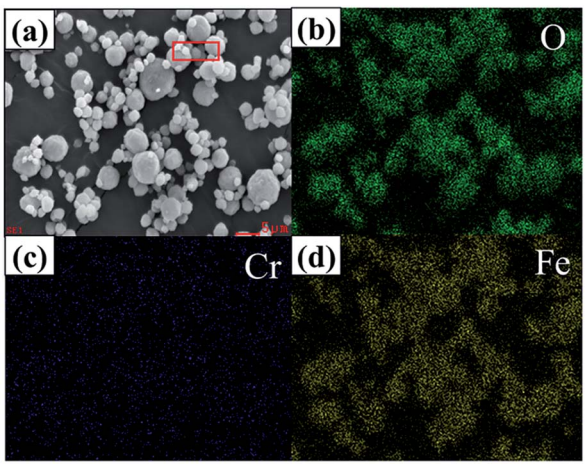

Fig. 3 EDS mapping of the $LiFe_{0.995}Cr_{0.005}BO_3/C$ sample: (a) sample images of the selective area (b) O, (c) Cr, (d) Fe.

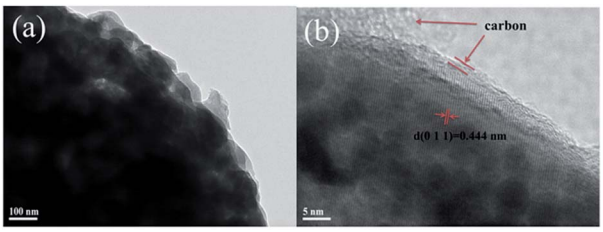

Fig. 4 (a and b) TEM images of the $LiFe_{0.995}Cr_{0.005}BO_3/C$.

Typical charge–discharge curves cycled in the voltage range between 1.5–4.5 V at ambient temperature conditions are shown in Fig. 5. The $LiFeBO_3/C$ can deliver an initial discharge specific capacity of 169.4 mA h g^{-1} at 0.1C (1C = 220 mA g^{-1}). The $LiFe_{0.995}Cr_{0.005}BO_3/C$ sample exhibits an initial discharge specific capacity of 196.3 mA h g^{-1} at 0.1C. This value is better than most previous reports.[4,13,15–17] The significant enhancement may result from the improvement of electronic/ionic conductivity of $LiFeBO_3/C$ by Cr doping.[19] However, the capacity increasing phenomenon is not maintained with further increase in Cr doping concentration. The discharge specific capacity for $LiFe_{0.992}Cr_{0.008}BO_3/C$ is 178.2 mA h g^{-1}. Therefore, the optimal Cr doping amount is 0.5% in the $LiFeBO_3/C$.

The cycling and rate performance of the $LiFeBO_3/C$ and $LiFe_{0.995}Cr_{0.005}BO_3/C$ samples are shown in Fig. 6(a) compares the cycling performances of $LiFeBO_3/C$ and $LiFe_{0.995}Cr_{0.005}BO_3/C$ at 1C. $LiFeBO_3/C$ can deliver an initial discharge specific capacity of 141.2 mA h g^{-1} with 89% capacity retention after 50 cycles at 1C. It is better than the result of the mesoporous

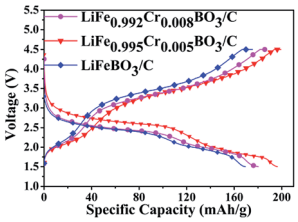

Fig. 5 Charge and discharge curves of the $LiFe_{1-x}Cr_xBO_3/C$ (x = 0, 0.005, 0.008) at 0.1C.

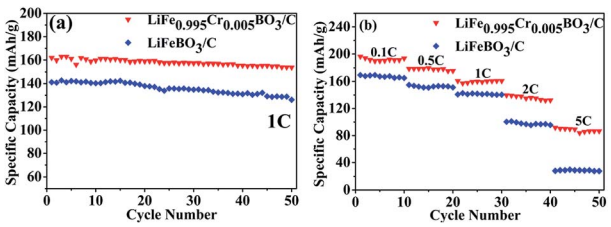

Fig. 6 (a) Cycling performances of the $LiFeBO_3/C$ and the $LiFe_{0.995}Cr_{0.005}BO_3/C$ at 1C, (b) cycling performance of the $LiFeBO_3/C$ and the $LiFe_{0.995}Cr_{0.005}BO_3/C$ at various rates from 0.1C to 5C.

hollow spheres $LiFeBO_3$/C, 139 mA h g^{-1} at 1C, reported by Chen *et al.*[13] Compared with $LiFeBO_3$/C, the $LiFe_{0.995}Cr_{0.005}BO_3$/C exhibits higher discharge specific capacity of 161.9 mA h g^{-1} with higher capacity retention of 95% after 50 cycles at 1C. It indicates that Cr doping could improve the cyclic stability of $LiFeBO_3$/C. The discharge capacity of the $LiFeBO_3$/C and $LiFe_{0.995}Cr_{0.005}BO_3$/C samples at various rate, *i.e.*, C/10, C/2, 1C, 2C and 5C, in the voltage range of 1.5–4.5 V are shown in Fig. 6(b). Overall, the discharge capacity of the $LiFe_{0.995}Cr_{0.005}BO_3$/C is higher than that of $LiFeBO_3$/C. With the discharge rate increasing, the superiority of the $LiFe_{0.995}Cr_{0.005}BO_3$/C becomes more pronounced. When the rate is as high as 5C, the discharge specific capacity of the $LiFe_{0.995}Cr_{0.005}BO_3$/C still remains 91.8 mA h g^{-1}. Chen *et al.* reported that nano-sized $LiFeBO_3$/C mesoporous hollow spheres delivered only a discharge specific capacity of 80 mA h g^{-1} at 4C.[13] While, the discharge specific capacity of the $LiFeBO_3$/C is only 28 mA h g^{-1} at 5C. The results confirmed that Cr doping could effectively enhance the rate performance of $LiFeBO_3$/C, which may contribute to the improvement of ionic conductivity.

To gain further insight into the essence of improvement in electrochemical properties, a comparison between the electric conductivity for the $LiFeBO_3$/C and $LiFe_{0.995}Cr_{0.005}BO_3$/C samples is shown in Fig. 7. The electric conductivity of $LiFe_{0.995}Cr_{0.005}BO_3$/C powder is calculated as 4.75×10^{-5} S cm^{-1}, while the value for $LiFeBO_3$/C powder is only 4.15×10^{-6} S cm^{-1}. Apparently, Cr doping can improve the electronic conductivity resulting in better electrochemical properties. The result was in accordance with the enhanced $LiFePO_4$ by Fe-site doping.[18]

In order to verify the influence of Cr doping on the Li ions diffusion coefficient, electrochemical impedance spectroscopy (EIS) measurements of $LiFeBO_3$/C and $LiFe_{0.995}Cr_{0.005}BO_3$/C were performed. Before EIS measurements, several preliminary galvanostatic cycles were performed for stable SEI film formation and the good permeation of the electrolyte into the active material. Fig. 8(a) shows the Nyquist and fitting plots of $LiFe_{0.995}Cr_{0.005}BO_3$/C and $LiFeBO_3$/C samples after 10 cycles at 0.1C, and the equivalent circuits shown in the inset of Fig. 8(a). As shown in Fig. 8(a), all the curves consist of a single semicircle in the high frequency region and an inclined line at low frequency region. The intercept on the Z' axis in the high frequency region corresponds to the ohmic resistance (R_s) of electrolyte, the semicircle in the high-to-medium frequency range is related to the charge transfer resistance (R_{ct}) on the interface of the electrolyte/electrode. As shown in Table 2, the simulation parameters of the equivalent circuit are obtained by electrochemical workstation (Autolab PGSTAT302N). The charge-transfer resistance (R_{ct}) of $LiFe_{0.995}Cr_{0.005}BO_3$/C electrode is 54.5 Ω, much smaller than that of the pristine $LiFeBO_3$/C (~215 Ω), indicating that the charge transfer at the electrolyte/electrode interface is greatly enhanced by Cr doping. The result is consistent with electric conductivity test (Fig. 7), which proved that the Cr doping can greatly improve the conductivity of $LiFe_{0.995}Cr_{0.005}BO_3$/C sample and thus enhance the electron transport during the lithiation/delithiation reaction. The sloping line at low frequency is associated with the diffusion in the solid phase. The lithium ion diffusion coefficient can be calculated from the formula (1) as following

$$D = \frac{R^2T^2}{2A^2n^2F^2C^2\sigma^2} \quad (1)$$

where R is the gas constant, T is the absolute temperature, n is the number of electrons transferred in the half-reaction for the redox couple, F is the Faraday constant, C is the concentration of lithium ion, σ is the slope of the line Z'–$\omega^{-1/2}$ which can be obtained from the line of Z'–$\omega^{-1/2}$ (show in Fig. 8b)

$$C = \frac{n}{V} = \frac{m/M}{V} = \frac{\rho V/M}{V} = \frac{\rho}{M} \quad (2)$$

where the constant values of F and R are 96 500 C mol^{-1} and 8.314 J K^{-1} mol^{-1}, respectively. A is the electrode area, which is 1.13×10^{-4} m^2, n is 1, T is 298 K, C can be calculated from the density and the molecular weight of the materials synthesized by different methods, which are 2.8×10^4 mol m^{-3} in our case.[22]

According to formula (1) and (2), Li ion diffusion coefficients (D_{Li}) of the $LiFeBO_3$/C and $LiFe_{0.995}Cr_{0.005}BO_3$/C are calculated separately, which are 5.92×10^{-14} cm^2 s^{-1} and 9.20×10^{-13} cm^2 s^{-1}. The D_{Li} of the $LiFe_{0.995}Cr_{0.005}BO_3$/C is about one order of magnitude higher than that of the pristine $LiFeBO_3$/C. It may be attributed to the chemistry defect in the lattice resulting from balancing the valence difference brought in by the Cr

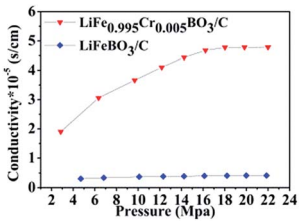

Fig. 7 The electronic conductivities of the prepared the $LiFeBO_3$/C and the $LiFe_{0.995}Cr_{0.005}BO_3$/C.

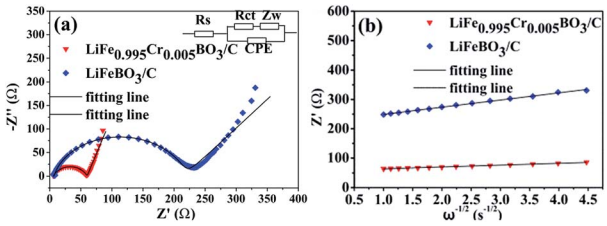

Fig. 8 (a) The EIS and fitting plots of the $LiFeBO_3$/C and the $LiFe_{0.995}Cr_{0.005}BO_3$/C after 10 cycles at 0.1C, (b) the relationship between Z' and $\omega^{-1/2}$ in low frequency.

Table 2 Electrode kinetic parameters obtained from equivalent circuit fitting of $LiFeBO_3$/C and the $LiFe_{0.995}Cr_{0.005}BO_3$/C

Electrode	R_s (Ω)	R_{ct} (Ω)	D (cm^2 s^{-1})
$LiFeBO_3$/C	6.65	215	5.94×10^{-14}
$LiFe_{0.995}Cr_{0.005}BO_3$/C	5.64	54.5	9.20×10^{-13}

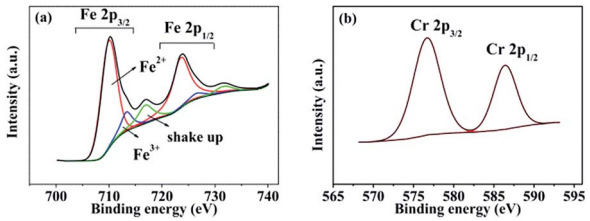

Fig. 9 (a) Fe 2p and (b) Cr 2p XPS spectra of the $LiFe_{0.995}Cr_{0.005}BO_3$/C.

doping.[23] The considerable improvement of the D_{Li} of $LiFeBO_3$/C directly leads to the enhancement of rate performance.

XPS measurements were performed to determine the chemical states of the $LiFe_{0.995}Cr_{0.005}BO_3$/C sample. Fig. 9(a) and (b) present the XPS spectra of the Fe 2p and Cr 2p, respectively. The Fe 2p orbital is clearly resolved into Fe ($2p_{3/2}$) and Fe ($2p_{1/2}$) contributions, centred upon 709.9 eV, 713.2 eV 723.4 eV and 725.9 eV, respectively. The binding energies 709.9 eV and 713.2 eV correspond to the characteristic peak of Fe^{2+} and Fe^{3+}, respectively. The apparent weak of shake up feature in high-resolution spectrum for Fe as shown in Fig. 9(a) suggests that all Fe atoms are in the structure of $LiFeBO_3$.[24] The content of Fe^{3+} is about 10%, which may contribute to the preparation process. The Cr 2p orbital is clearly resolved into Cr ($2p_{3/2}$) and Cr ($2p_{1/2}$) contributions, centred upon 576.7 eV, 586.4 eV. The peak of 576.7 eV in Cr ($2p_{3/2}$) corresponds to the characteristic peak Cr^{3+}. Owing to the supervalent Cr^{3+} is doped in $LiFeBO_3$ at Fe sites, Fe vacancies would be produced to balance the valence.[25] The following short equation (using Kröger–Vink notation[26]) describes the valence balance model:

$$\frac{1}{2}Cr_2O_3 + \frac{3}{2}Fe_{Fe}^{\times} \rightarrow Cr_{Fe}^{\cdot} + \frac{1}{2}V_{Fe}^{''} + \frac{3}{2}FeO \quad (3)$$

Cr doping increases the concentration of ionic vacancies according to formula (3). Basing on formula (3), two Cr atoms could substitute three Fe atoms. Thus, to maintain neutrality of the lattice in $LiFeBO_3$, conduction electrons are produced locally to balance the Cr^{3+}.[27] It facilitates the Li ion diffusivity and electron conduction during the charge–discharge process.[19,20]

4. Conclusions

$LiFe_{1-x}Cr_xBO_3$/C ($x = 0$, 0.005, 0.008) were prepared by *via* ball-milling and spray-drying assisted high-temperature solid-state reaction. Cr element was proved to disperse uniformly in the samples and enter the structure of the monoclinic $LiFeBO_3$ forming a solid solution. In the SEM and TEM images, $LiFe_{0.995}Cr_{0.005}BO_3$ particles were covered by amorphous carbon layer, which form a conductive network. It was found that Cr doping played an important role in promoting the electrochemical performance. $LiFe_{0.995}Cr_{0.005}BO_3$ showed the highest discharge capacity of 196.3 mA h g^{-1} at 0.1C, which was 26.9 mA h g^{-1} higher than that of the $LiFeBO_3$/C. The cyclic retention of $LiFe_{0.995}Cr_{0.005}BO_3$/C was 95% after 50 cycles at 1C, which was much better than that of the $LiFeBO_3$/C (89%). Cr doping improved the rate performance of the $LiFeBO_3$/C as well. The discharge capacity of the $LiFe_{0.995}Cr_{0.005}BO_3$/C was 91.8 mA h g^{-1} at 5C, which was 3.27 times than that of the $LiFeBO_3$/C (28 mA h g^{-1}). The electrochemical performance improvement of the $LiFeBO_3$/C by Cr doping was attributed to both the high electronic conductivities (4.75×10^{-5} S cm^{-1}) and fast Li ion diffusion coefficients (9.20×10^{-13} cm^2 s^{-1}) of the $LiFe_{0.995}Cr_{0.005}BO_3$/C. Basing on the XPS results, the mechanism of Cr doping was analysed. The supervalent Cr^{3+} doping would produce Fe vacancies with accompanying conduction electrons to maintain neutrality of the lattice in $LiFeBO_3$, which lead to the improvement of electronic conductivities and D_{Li}.

Acknowledgements

We gratefully acknowledge the financial support by the Innovation Program of Shanghai Municipal education commission (15ZZ095) and the Science and Technology Commission of Shanghai Municipality (14520503100).

References

1 Z. A. Zhang, Z. Y. Zhang, W. Chen, G. C. Wang, *et al.*, *New J. Chem.*, 2015, **39**, 3765–3769.
2 J. C. Zheng, Y. D. Han, D. Sun, B. Zhang and E. J. Cairns, *Energy Storage Materials*, 2017, **7**, 48–55.
3 A. P. Tang, D. H. He, Z. Q. He, G. R. Xu, *et al.*, *J. Power Sources*, 2015, **275**, 888–892.
4 B. Zhang, L. Ming, J. C. Zheng, J. F. Zhang, *et al.*, *J. Power Sources*, 2014, **261**, 249–254.
5 Y. Z. Dong, Y. M. Zhao, Z. D. Shi, X. N. An, P. Fu and L. Chen, *Electrochim. Acta*, 2008, **53**, 2339–2345.
6 K. Wang, W. j. Ren, J. L. Yang, R. Tan, Y. D. Liu and F. Pan, *RSC Adv.*, 2016, **6**, 47723–47729.
7 L. Sebastian and J. Gopalakrishnan, *J. Solid State Chem.*, 2003, **172**, 171–177.
8 V. Legagneur, Y. An, A. Mosbah, R. Portal, *et al.*, *Solid State Ionics*, 2001, **139**, 37–46.
9 A. Yamada, N. Iwane, Y. Harada, S. I. Nishimura, Y. Koyama and I. Tanaka, *Adv. Mater.*, 2010, **22**, 3583–3587.
10 S. H. Bo, F. Wang, Y. Janssen, D. Zeng, K. W. Name, W. Xu, L. S. Du, J. Graetz, X. Q. Yang, Y. Zhu, J. B. Parise, C. P. Grey and P. G. Khalifah, *J. Mater. Chem.*, 2012, **22**, 8799–8809.
11 P. Barpanda, Y. Yamashita, Y. Yamada and A. Yamada, *J. Electrochem. Soc.*, 2013, **160**, A3095–A3099.
12 L. Tao, G. Rousse, J. N. Chotard, L. Dupont, *et al.*, *J. Mater. Chem. A*, 2014, **2**, 2060–2070.
13 Z. X. Chen, L. F. Cao, L. Chen, H. H. Zhou, C. M. Zheng, *et al.*, *J. Power Sources*, 2015, **298**, 355–362.
14 J. C. Zheng, S. E. Qin, B. Zhang, X. Ou, L. Ming and C. Shen, *Chem. Lett.*, 2014, **43**, 1411–1413.
15 A. Yamada, N. Iwane, S. I. Nishimura, Y. Koyama and I. Tanaka, *J. Mater. Chem.*, 2011, **22**, 10690–10696.
16 Z. P. Li, Y. P. Wang, Q. R. Hu, Y. Yang, Z. C. Wu and C. M. Ban, *J. Nanosci. Nanotechnol.*, 2015, **15**, 7186–7190.

17 M. A. Cambaz, M. A. Reddy, B. P. Vinayan, R. Witte, *et al.*, *ACS Appl. Mater. Interfaces*, 2016, **8**, 2166–2172.
18 D. Y. Wang, H. Li, S. Q. Shi, X. J. Huang and L. Q. Chen, *Electrochim. Acta*, 2005, **50**, 2955–2958.
19 C. K. Park, S. B. Park, H. C. Shin, W. Cho and H. Jang, *Bull. Korean Chem. Soc.*, 2011, **32**, 191–195.
20 H. C. Shin, S. B. Park, H. Jang, K. Y. Chung, W. I. Cho, C. S. Kim and B. W. Cho, *Electrochim. Acta*, 2008, **53**, 7946–7951.
21 Y. X. Wen, L. M. Zeng, Z. F. Tong, L. Q. Nong and W. X. Wei, *J. Alloys Compd.*, 2006, **416**, 206–208.
22 X. Y. Wang, H. Hao, J. L. Liu, T. Huang and A. S. Yu, *Electrochim. Acta*, 2011, **56**, 4065–4069.
23 Y. Gan, C. Chen, J. L. Liu, P. W. Bian, H. Hao and A. S. Yu, *J. Alloys Compd.*, 2015, **620**, 350–357.
24 L. Y. Liu, Y. Cheng, Z. F. Liu, M. N. Ha, Q. S. Quo and Z. Zhao, *RSC Adv.*, 2016, **6**, 83814–83829.
25 N. Meethong, Y. H. Kao, S. A. Speakman and Y. M. Chiang, *Adv. Funct. Mater.*, 2009, **19**, 1060–1070.
26 F. A. Kröger and H. J. Vink, *Solid State Phys.*, 1956, **3**, 307–435.
27 K. Haffe, *Oxidation of Metals*, Plenum Press, 1965.